



Project no. TIP5-CT-2006-031415

## INNOTRACK

Integrated Project (IP)

Thematic Priority 6: Sustainable Development, Global Change and Ecosystems

### D4.3.4 - Calculation of contact stresses for laboratory test rigs

Due date of deliverable: 2008/09/30

Actual submission date: 2009/02/15

Start date of project: 1<sup>st</sup> of September 2006

Duration: 36 months

Organisation name of lead contractor for this deliverable:

TU Delft

Revision Final

Project co-funded by the European Commission within the Sixth Framework Programme (2002-2006)		
Dissemination Level		
<b>PU</b>	Public	X
<b>PP</b>	Restricted to other programme participants (including the Commission Services)	
<b>RE</b>	Restricted to a group specified by the consortium (including the Commission Services)	
<b>CO</b>	Confidential, only for members of the consortium (including the Commission Services)	

# Table of Contents

---

<b>Table of figures</b> .....	<b>3</b>
<b>Glossary</b> .....	<b>4</b>
<b>1. Executive Summary</b> .....	<b>5</b>
<b>2. Introduction</b> .....	<b>6</b>
<b>3. A short description of the test rigs</b> .....	<b>7</b>
3.1 The SUROS machine .....	7
3.2 The test rig of VAS .....	7
3.3 The DB test rig C .....	8
<b>4. A methodology for wheel-rail rolling contact simulation</b> .....	<b>10</b>
4.1 Introduction.....	10
4.2 Motion of a wheelset along track.....	10
4.3 Search of contact points between wheels and rails .....	10
4.4 Two local coordinate systems .....	12
4.5 Kalker theory .....	13
4.6 Non-Hertzian contact.....	14
4.6.1 <i>Conformal contact</i> .....	16
4.6.2 <i>Two-point contact and multiple-point contact</i> .....	16
<b>5. Simulation of the lab tests</b> .....	<b>18</b>
5.1 The UoN test results.....	18
5.2 The VAS test .....	19
5.3 The DB rig C test.....	19
5.4 Comparison of results of the three rigs .....	19
5.5 Some further discussions .....	20
<b>6. Conclusions</b> .....	<b>21</b>
<b>7. References</b> .....	<b>22</b>
<b>8. Annexes</b> .....	<b>23</b>

## Table of figures

---

Figure 1 - The cylindrical contact of the SUROS machine. From [1].....	7
Figure 2 - Wheel-rail contact on the VAS rig. From [1], with location of Q modified to reflect the actual test situation .....	8
Figure 3- The DB test rig. From [1].....	9
Figure 4 - The motion of wheelset relative to track .....	11
Figure 5 - Surface discretization and the two local coordinates systems .....	12
Figure 6 - Various rolling contacts solved by Kalker [3] .....	14
Figure 7 - Hertzian contact versus non-Hertzian contact .....	15
Figure 8 - Non-Hertzian contact solution can automatically taken 2-point or multiple-point contact. ....	15
Figure 9 - Normal pressure changes when a wheel-rail contact transits from tread-rail top contact ( $\Delta y \leq 7.50\text{mm}$ ) to flange-gage corner contact ( $\Delta y \geq 7.96\text{mm}$ ). Calculated by WEAR. ....	17
Figure 10 - Tangential traction distribution between rolling cylinders. $a$ is the semi-width of the rectangular contact area. The area $[-a, l]$ is in slip, while $[l, a]$ is in adhesion. ....	18
Table 1 - maximal shear stress and locations calculated (in GPa) .....	19

## Glossary

---

<b>Abbreviation / acronym</b>	<b>Description</b>
CONTACT	A computer program for solving rolling contact problems. Developed at TU Delft
FEM	Finite element method
HC	Head checks or head checking, a major type of RCF
KMS	Knowledge management system
Miniprof	A portable device for measurement of transverse profiles of wheels and rails
RCF	Rolling contact fatigue
SP	Sub Project
WEAR	A computer program for simulation of rolling contact and wear. Extended from CONTACT and developed at TU Delft
SUROS	Sheffield University Rolling Sliding test rig (Twin disc)
WP	Work Package
Chalmers	Chalmers University of Technology, Göteborg
DB	Deutsche Bahn Technik/Beschaffung
TUD	Technical University Delft
UoN	University of Newcastle
VAS	Voestalpine Schienen GmbH

# 1. Executive Summary

---

In this report a methodology for the simulation and analyses of wheel-rail rolling contact is presented. It is applied to the determination of the contact stress, micro-slip and the location of maximal contact stress of the first laboratory tests conducted in the frame of WP4.3. Subsequently the locations of RCF initiation are predicted. The predictions are compared with the test results, and the validity of the methodology is established. It is also shown that with the presented methodology deviation of rolling contact conditions from their nominal ones can be identified, so that accurate predictions can be made.

The methodology can be employed for analysis of rolling contact under operational conditions and lab conditions. The results of the analyses can further be used for wear and rolling contact fatigue analyses etc.

The report D4.3.4 was undertaken to support comparison of contact conditions between the machines used for testing within WP 4.3

## 2. Introduction

---

The overall objectives of Work Package (WP) 4.3 are (see *Detailed Implementation Plan D4* (Document name in KMS is *int-sp43-19-150802-d4-dip\_next\_18\_months[1].doc*):

- Design innovative laboratory tests of rail steel grades and joints.
- Perform experimental work on wheel-rail stresses, wear and crack initiation to generate wear and cracking data under controlled operating conditions.
- Installation of laboratory tests to fill the gaps of knowledge detected and relevant for LCC's
- Comparison of laboratory tests with numerical RCF predictions

In the meeting of 28<sup>th</sup> of February, 2007, it was decided to perform the tests on the SUROS twin-disc machine of University of Sheffield, the VAS linear rig and the DB Rig C, see [1].

This deliverable is a step towards the second and the fourth objectives. It is undertaken for the second objective to compare the contact conditions between the test rigs used for WP 4.3. By comparing the predictions with the test results the validity of the numerical methods may be proven (objective 4). The following quantities are expected for subsequent WP4.3 analyses:

- Normal and tangential tractions in the contact area of the different test rigs
- Location of the maximum pressure/maximum shear stress
- Micro-slip

To such ends the lab tests were simulated. Data were obtained from laboratory tests on three rigs with different settings and complexities, see references [1] and [2], varying from the simple twin-disc to the wheelset-on-rollers rig. The latter is, in terms of rolling contact constraints, equivalent to the wheelset-track interaction under operation conditions. The simulation and analysis methodology is therefore introduced in the frame of a general wheelset-track interaction system. Such a simulation includes the search of the contact points and the solution of the contact problems in the vicinity of the contact points. The former takes the influence of parameters such as wheel/rail lateral relative position, rail inclination and angle of attack into account. The later includes the determination of the contact areas, the normal and tangential surface stress distributions, the micro-slip in the contact interface and the locations of the maximal pressure and shear stress.

It is emphasized that the determination of the contact conditions involves both the global wheelset-track interaction and the local contact. These concern two distinctive subjects: vehicle dynamics and contact mechanics, each of them has its own terminology, reference coordinate systems and conventions. In this report attempts are made to unify them for the purpose of this deliverable. It is, however, not a general discussion of the two subjects, though the methodology presented is applicable to general wheelset-track interaction, because that a rigorous general discussion of such subjects demands a much larger text, and is out of the scope of this deliverable.

It is emphasised that this deliverable should be read in conjunction with other documents of WP4.3, see references [1, 2], to obtain a full understanding of the test methodology and the results.

It should also be noted that initially it was intended to include a wear model in this deliverable. It was decided in the WP4.2 meeting held on 24<sup>th</sup> of November, 2008 in Brussels at UNIFE to moved it to deliverable D4.2.5

### 3. A short description of the test rigs

---

To provide background for the conditions under which the wheel-rail contact stresses and wear will be calculated, a short description of the test rigs selected in the test matrix is presented. More details can be found in [1, 2]

#### 3.1 The SUROS machine

UoN used the SUROS machine of the University of Sheffield for WP4.3. The contact of the SUROS twin-disc machine is between two cylindrical discs, as shown in Figure 1. Vertical and longitudinal (in rolling direction) loading can be applied.



*Figure 1 - The cylindrical contact of the SUROS machine. From [1]*

#### 3.2 The test rig of VAS

At the VAS rig it is a real wheel rolling on a real rail. Vertical and lateral load can be applied. The rail inclination and angle of attack can be adjusted. The vertical load is applied on the wheel axle and the lateral force  $Q$  is applied on the rail. The wheel rolls over the rail along direction  $T$ .

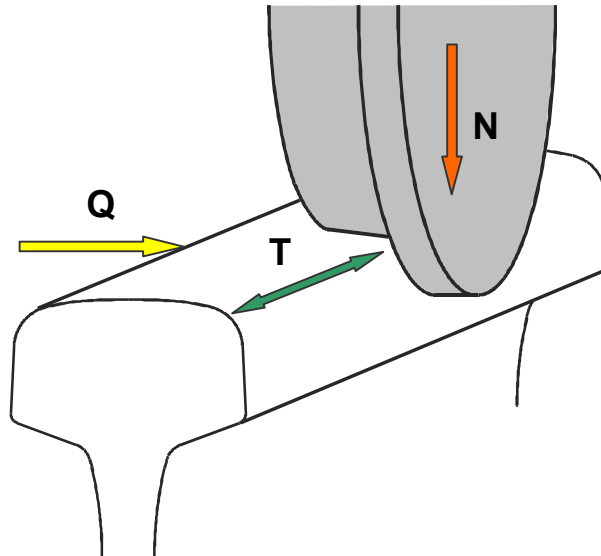


**Figure 2 - Wheel-rail contact on the VAS rig. From [1], with location of Q modified to reflect the actual test situation**

### 3.3 The DB test rig C

The DB test rig C, which is used for WP4.3 has a wheelset-on-roller contact. See **Error! Reference source not found.** As the rail profile (of the rollers) is not inclined, one wheel bearing has to be lifted by about 50 mm in order to obtain an effective rail inclination of 1:40. The angle of attack is simulated by turning the wheelset about the vertical axis against the gauge corner in the rolling direction as shown in **Error! Reference source not found.**

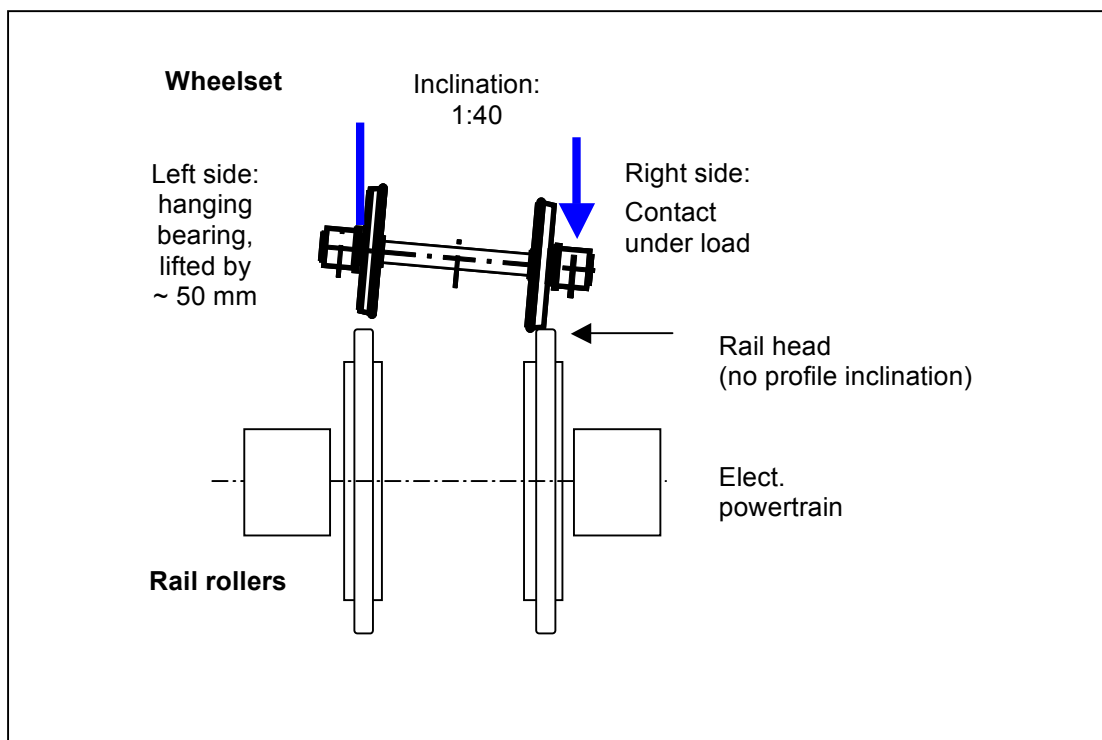


**Figure 3 (a) - Inclined wheelset to simulate rail inclination (front view)**

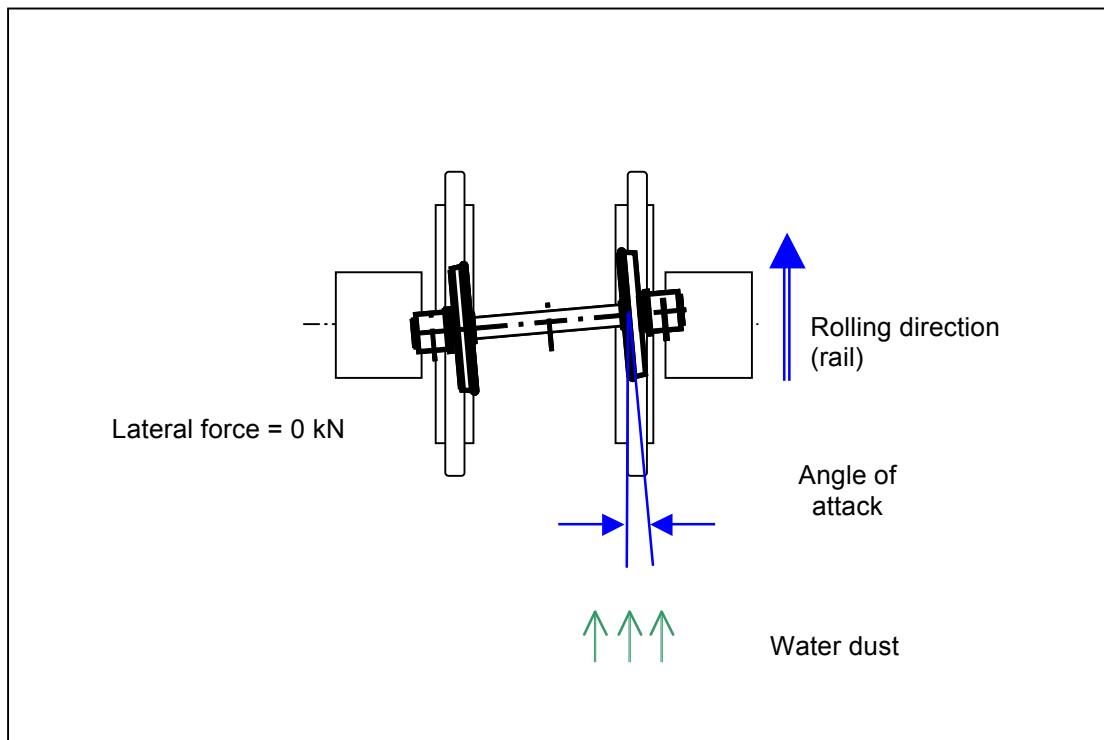


**Figure 3 (b) - Simulation of angle of attack at the roller rig (top view)**

**Figure 3- The DB test rig. From [1]**

## 4. A methodology for wheel-rail rolling contact simulation

---

### 4.1 Introduction

Under operation conditions it is two wheels mounted on an axle as a wheelset roll along the track. Simulation of the rolling contact includes the search of the contact points between the wheels and the rails, and solution of the contact problems in the vicinity of the contact points. In this chapter the search of contact points is first briefly discussed, taking into consideration of the possible motion of a wheelset along a track. Subsequently solution methods for the contact problems are presented. Kalker's variational and numerical solution [3] is employed where it is applicable. At flange-gage corner contact Kalker's solution is extended to take into account of the conformity and the associated large (geometrical) spin creepage [4].

The whole procedure is integrated and implemented in the computer code WEAR. Tests on the three rigs can be simulated by WEAR as a special case of wheelset-track interaction. In the discussion that follows in this chapter, the discs, roller, wheel and rail are generally referred to as wheel and rail according to their respective function on the respective rigs.

### 4.2 Motion of a wheelset along track

The location of wheel-rail contact is defined in the track coordinate system XYZ. The origin of the system is on the centre line of the track in the plane tangent to the top of the two rails, with X-axis tangent to the track centre line and pointing to the forward direction of the wheelset. Z points downward. Y is so defined that XYZ forms a right-handed Cartesian coordinate system. The independent variables of the wheelset motion along the track is the wheelset lateral displacement  $\Delta Y$  and the yaw angle  $\psi$ , see figure 4. In wheelset-track interaction, there is another motion of the wheelset, roll  $\theta$ , which is dependent upon  $\Delta y$  and  $\psi$ , see figure 4(c), due to the constraining of the track. In the lab tests,  $\theta$  is kept constant by design.

### 4.3 Search of contact points between wheels and rails

To solve a wheel-rail contact problem, an important first step is to find the locations of the contact points between the wheels and rails. The search is in the wheelset-track system, with  $\Delta Y$  and  $\psi$  being the independent variables. It should be pointed out that rail inclination, and in the case of the DB test rig C the wheelset inclination, affects greatly the location of the contact points. Their effect is taken into account by rotating the profiles of the rails or wheels accordingly in the direction it is inclined. For this search the wheelset and rails are considered as rigid bodies for the search of the contact points. The contact points found are therefore called rigid body contact points. Contact areas form at these contact points as a result of deformation. Usually one rigid body contact is found at each of the two wheel-rail couples. Two-point rigid body contact may often be found when flange contact is involved.

The algorithm for the search of the rigid body contact points was presented in [6]. In application to wear simulation in [5], where wear of wheel profile caused excessive wheelset hunting, the algorithm was validated in the following ways: The search was performed with WEAR and with Simpack<sup>1</sup> separately by the different co-authors of [5], with all the conditions being the same; their results agreed with each other. It was further validated in the sense that the simulated wear was in agreement with the measured wear of the wheels and that the simulated wheel hunting frequency based on the simulated wear agreed with the hunting frequency observed in field [5].

---

<sup>1</sup> Simpack is a widely accepted multi-body simulation software package.

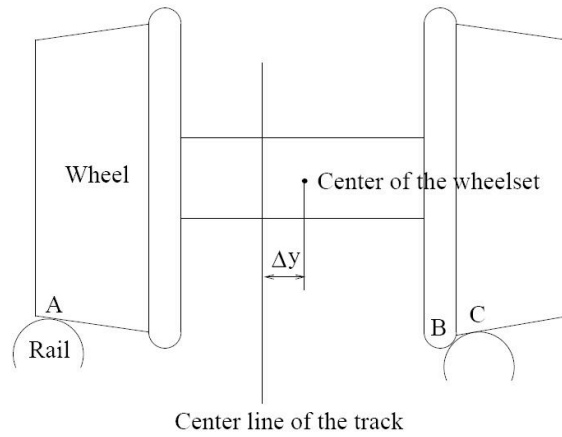


**Figure 4 (a) - Lateral displacement of wheelset with respect to the track centre  $\Delta Y$**

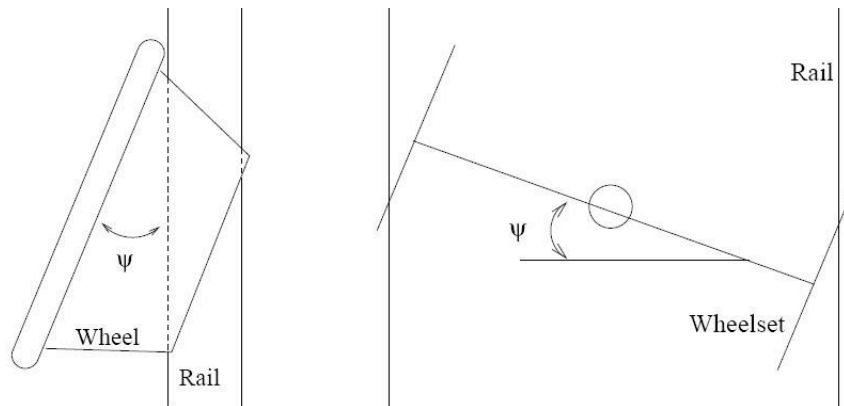


**Figure 4 (b) - Yaw angle (Angle of attack)  $\psi$  is the angle between wheelset axis and the tangent of the track centre line**

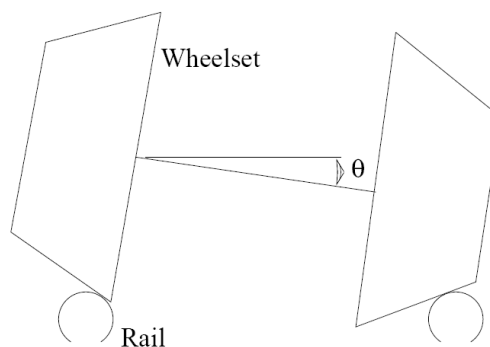


**Figure 4 (c) - Roll angle  $\theta$  is the angle between the wheelset axis and the track plane. It is not an independent variable, but is a function of  $\Delta y$  and  $\psi$ .**

**Figure 4 - The motion of wheelset relative to track**

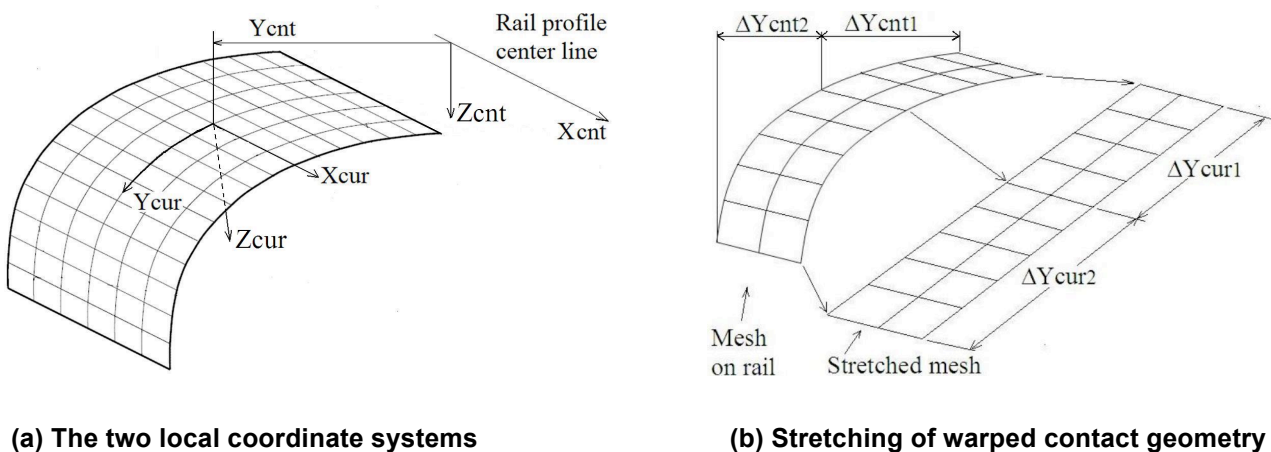
Wheelset and rail, including the test rigs, are in reality deformable. Under large load the deformation may not be negligible for the determination of the location of contact points. Such deformation may be determined by

analyzing the contact conditions with WEAR and taken into account in subsequent analyses. The deformation and their effects are discussed and considered in this report.

## 4.4 Two local coordinate systems

For a complete description of a wheel-rail contact, two additional local coordinate systems are needed besides the global track coordinate system introduced in section 4.2. The first one is the right-handed Cartesian rail coordinate system  $X_{cnt}Y_{cnt}Z_{cnt}$ , see figure 5(a). Its origin is at the centre of the rail profile, which is so defined that it has equal horizontal distances to the two ends of the profile when the rail is not inclined. If the profile changes due to wear or deformation during an analysis, the centre point is usually chosen on the initial profile. That initial profile may be called the reference profile.  $X_{cnt}$  points to the rolling direction,  $Y_{cnt}$  points to the gage side and is horizontal when the rail is not inclined.  $X_{cnt}Y_{cnt}Z_{cnt}$  rotates together with the profile if the rail is inclined.

The other coordinate system is the discretization coordinate system  $X_{cur}Y_{cur}Z_{cur}$ , see figure 5(a). It is a curvilinear system, needed for the discretization and solution of a contact problem. Its origin is at the rigid body contact point.  $X_{cur}$  points to the rolling direction.  $Y_{cur}$  is tangent to the local profile and points to the gage side.  $Z_{cur}$  is normal to the local rail surface, pointing into the rail. Note that  $X_{cur}Y_{cur}Z_{cur}$  applies also to the general geometry shown in figure 7.



**(a) The two local coordinate systems** **(b) Stretching of warped contact geometry**  
**Figure 5 - Surface discretization and the two local coordinates systems**

In section 4.2 and in this section three coordinate systems are introduced. The relation between them is as follows.

The track coordinate system XYZ provides a reference for the motion of a wheelset relative to the track. In this coordinate system the locations of the rigid body contact points are determined, and are converted into  $Y_{cnt}$  in the rail coordinate system, and designated as  $Y_{cnt\ rig}$ . This conversion is necessary because the locations of contact points and HC are most conveniently measured on the rail, not from the track centre. It is noted that the  $Y_{cnt\ rig}$  is usually not equal to the corresponding  $\Delta Y$ .

In the rail coordinate system,  $Y_{cnt}$  is measured from the centre of the reference rail profile. This is necessary because it provide a fixed coordinate origin even if the profile changes due to wear or deformation. In practice a point on the rail is most conveniently measured from the rail side. Therefore a conversion needs to be made between the results of WEAR and of measurement. If the rail gage face is not severely worn, the conversion can approximately be

$$\text{Location of rigid body contact point measured from inner/gage side of rail} = \text{half of rail head width} - Y_{cnt\ rig}$$

If the gage face is severely worn, a reasonably accurate conversion has to be made by comparing the worn profile with the reference profile.

The solution of a contact problem is obtained in the curvi-linear system, but the locations of the stress and micro-slip need to be converted into the rail coordinate system for comparison and discussion, because their distributions are more conveniently measured and visualised on a flat surface than on an arbitrary curved surface. Figure 5(b) shows schematically the conversion between  $X_{cnt}Y_{cnt}Z_{cnt}$  and  $X_{cur}Y_{cur}Z_{cur}$ , and how by the conversion a warped surface is stretched into being flat. It is noted that on the rail top the difference between  $\Delta Y_{cnt1}$  and  $\Delta Y_{cur1}$  is perhaps not so significant, and sometimes can be ignored, while at the gage face the difference between  $\Delta Y_{cnt2}$  and  $\Delta Y_{cur2}$  can be very large. An example is given in section 6.1 of annex 3 for the conversion of a warped contact area on to a flat surface. In figure 9 the pressure is plotted over the stretched (flat) contact areas.

## 4.5 Kalker theory

The contact on the SUROS machine is a special case of Hertzian contact - a line contact. This is the case where one dimension of the Hertzian ellipse is infinitely long, and has a simpler mathematical formulation. For such contact, the Carter theory is sufficient.

For the wheel-rail contact, Kalker's theories [3] have usually been employed. Kalker's theories are accepted worldwide for solution of wheel-rail rolling contact. Their correctness, accuracy, effectiveness and efficiency have been proven by many lab tests, numerous successful applications to railway vehicle dynamics and to analyses of rolling contact stress and strain. Figure 6 shows some results by Kalker [3]. Though for the present calculation of contact stress and micro-slip the finite element method (FEM) may be employed, the variational and numerical theory of Kalker (Chapter 4 of [3]), which is in the sequel referred to for short as the Kalker theory, is chosen for the sake of computational efficiency.

The Kalker theory is based on elasticity, statics, half-space approximation and Coulomb friction. For its applications to the present investigation in stress and micro-slip, elasticity can be justified because HC occurs only after many thousands of contacts so that for each contact cycle the component of plastic strain should be negligible compared to the total strain. In other words, elasticity is dominant. Statics is applicable because the occurrence of HC is basically a (quasi-) static process. This is based, among other arguments, on the fact that the majority of HC takes place on curves, the associated wavelength of the dynamic wheel-rail relative motion is a few meters or larger, while the dimension of a wheel-rail contact area is in the order of one centimetre and therefore much less than the wavelength of the wheelset. Hence the dynamic effect is negligible.

The Kalker theory has been implemented in his computer code CONTACT in the surface mechanics form. It means that the solution is sought on the wheel and rail surfaces, while the effect of the bulk materials on the relation between surface stress and displacement is taken into account by the so called influence numbers, which are calculated based on the Bossinesq-Cerruti solution for half-space [3]. For most situations half-space approximation is sufficient because the contact area is usually flat and small compared to the contacting surfaces of the wheel and the rail. Note that Hertz theory is also based on half-space assumption. The applicability of half-space assumption and a replacement of it are discussed in section 4.6.1. To drop the half-space approximation, FEM may have to be employed.

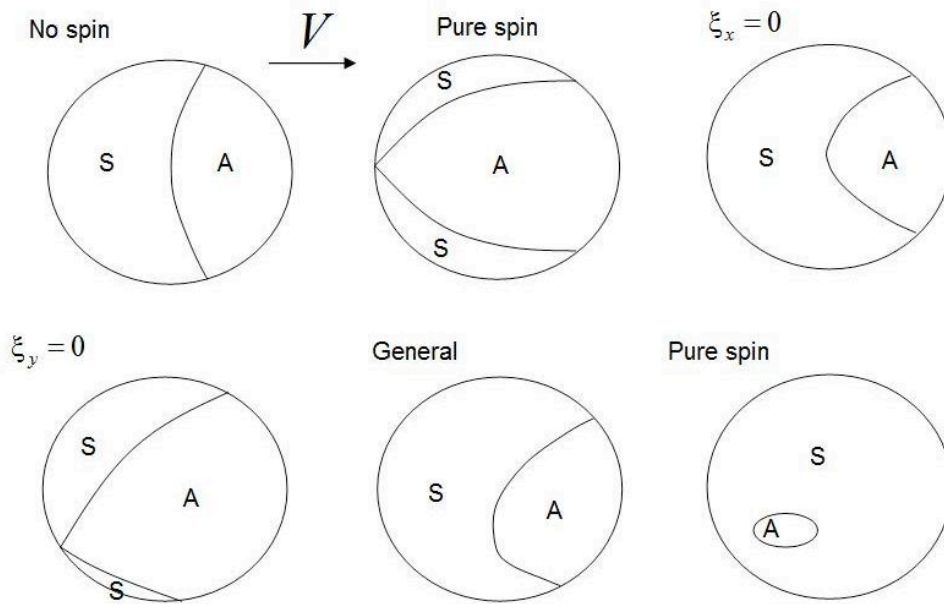


**Figure 6 - Various rolling contacts solved by Kalker [3]**

**The circles are normalized contact area. A indicates adhesion area, and S indicates slip area.  $\xi_x$  and  $\xi_y$  are the longitudinal (in rolling direction) and lateral creepages.  $V$  is velocity.**

## 4.6 Non-Hertzian contact

At this point some definitions should first be clarified. Hertz theory solves with known normal force and quadratic surface for contact area and pressure distribution, which turns out to be elliptical and semi-ellipsoidal, respectively; no friction is considered.

Rolling contact usually involves the solution of both the normal problem for the contact area and the pressure, and the tangential problem for the shear stress, the micro-slip and the division between the stick area and the slip area in the contact. The tangential problem is usually more difficult to solve. If the normal problem of a contact is solved with Hertz theory, the solution and the employed method is called Hertzian, though its tangential problem has still to be solved by some other means. If the normal problem can not be solved with Hertz theory, it is non-Hertzian.

For Hertzian problems each contacting surface may only be expressed with two principal radii of curvature at the rigid body contact point, see figure 7. Measured profiles have to be very well smoothed and are usually expressed in spline function to obtain the required radii. Such radii may sometimes only be able to characterize the very local geometry at the contact points, i.e. not the geometry in the entire contact area. This idealization may lead to lose of the real geometry, see figure 7 and 8 for illustration. For this deliverable, non-Hertzian solution is employed for the following reasons:

1. At gage corner, where HC often occurs, the contact is often very much conforming and two-point or even multiple-point contact may often occur.
2. For Hertzian contact only one transversal radius of curvature may be used for a rail or a wheel, while in reality, and particularly for worn profiles, the transverse radius varies continuously throughout the contact area.

For a comparison of the solutions of the same problems by Hertzian and non-Hertz methods, see annex 1 (*Hertzian solution vs non-Hertzian solution*).

Because Hertzian solution uses analytical quadratic geometry, the calculated surface stress distribution will be smooth. For a non-Hertzian solution of wheel-rail contact discrete points are used to represent the profiles; the stress distribution may therefore be less smooth, especially when the profiles are measured. The non-smoothness may be due to two causes: The first is that the real geometry is indeed not smooth. The second is owing to the error in the measurement. It is well known that profiles measured by a Miniprof<sup>2</sup> may have error up to 0.1 mm, while the usual compression of wheel-rail contact is also in the same order. For this deliverable piece-wise profile smoothing is performed with least square method using orthogonal polynomials, see annex 2 (*Profile Smoothing Method*).

Below further discussed are two typical types of wheel-rail non-Hertzian contact which are of importance for this deliverable.

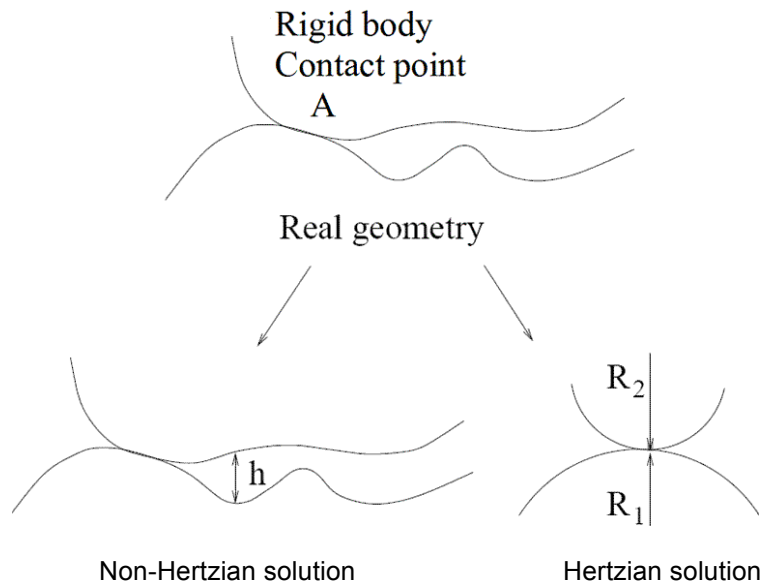


**Figure 7 - Hertzian contact versus non-Hertzian contact**

Different handling of contact geometry by the Hertz theory and by a non-Hertzian solution method. Real contact geometry on the upper plot is approximated in the Hertz solution with principal radii  $R_1$  and  $R_2$  in the transversal-vertical plane (i.e. in-plane with the wheel and rail profiles in the case of a zero yaw angle). In the longitudinal-vertical plane are the other two principal radii: namely the wheel rolling radius at the contact point and the rail radius which is usually taken as being infinite) at the rigid body contact point A. In non-Hertzian solution, the contact geometry is dealt with as it is. The distance  $h$  between the contacting surfaces as a location dependent variable replaces the role of the principal radii.

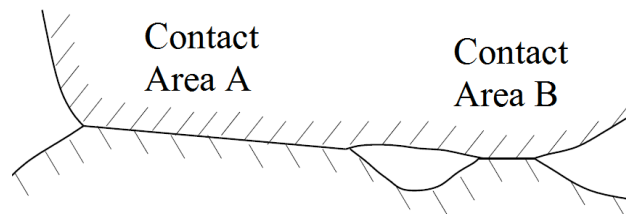


**Figure 8 - Non-Hertzian contact solution can automatically taken 2-point or multiple-point contact.**

<sup>2</sup> Miniprof is a type of devices which can measure the transverse profiles of wheels and rails.

The figure shows that the contact geometry given in the upper plot of figure 6 may result in a two-point contact if the normal load is high enough, with one contact area being at the rigid body contact point A, and another at contact area B.

#### 4.6.1 Conformal contact

For the case of wheel-rail conformal contact, where the applicability of half-space approximation may be argued, the algorithm of CONTACT is extended in WEAR. WEAR includes all the features of CONTACT, while for conformal contact improvements are made by replacing half-space with quasi-quarter spaces to better simulate wheel-rail gage corner contact [6]. The geometrical spin is fully accounted for. The influence numbers for the quasi-quarter space are obtained with the Finite Element Method.

As mentioned above the solution is obtained in the surface mechanical form. It means that the discretization is performed on the surfaces of the wheel and rail. Figure 5(a) shows a typical situation for contact at gage corner. The discretization is made on an estimation of the potential contact area, which should be large enough to include the entire contact area, while as small as possible to minimize the computational costs. WEAR estimates the potential contact area and perform the discretization automatically. It is noted that this discretization procedure is applied not only to the conformal contact, but to general wheel-rail contacts.

#### 4.6.2 Two-point contact and multiple-point contact

Two-point and multiple-point contact may take place between wheel and rail, especially at the transition between tread-rail head contact and flange-gage corner contact. By nature two-point and multiple-point contact are non-Hertzian<sup>3</sup>. Because HC occurs at the gage shoulder and gage corner, and two-point contact has usually significantly effect on the wear and RCF behaviour of rails, the solution method should be able to treat it accurately.

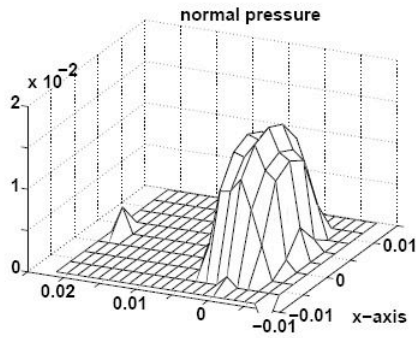
WEAR automatically detects and solve each two-point or multiple-point contact as one non-Hertzian problem [6]. Figure 9 shows the normal stress distribution when a wheel-rail two-point contract transits from tread-rail top contact to flange-gage corner contact.

---

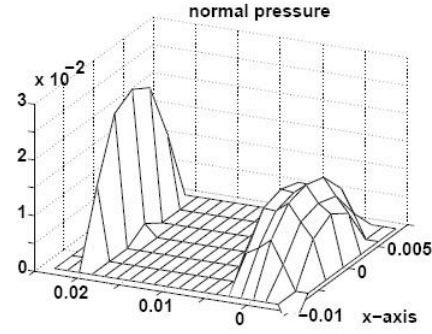
<sup>3</sup> A wheel-rail two- or multiple-point contact problem can usually not be solved with a Hertzian method because mathematically the problem is indeterminate. Take the solution of the normal problem of a two-point contact for example: There are two contact points. Hence there are, if to solve in a Hertzian manner, two Hertzian problems to treat separately on one wheel. But for each wheel there is only one known total normal force which is applied simultaneously on both points, see figures 2 and 3(a) for the application of the forces, through which the stress fields of the two Hertzian problems are coupled. The problem is therefore indeterminate, and can not be solved in a Hertzian way.

It is noted that sometimes in the solution of some two-point contacts, the contact area and pressure at one or both of the contact points may look like Hertzian. Figure 9 could be such a case for some readers. But for the reason given here above, the contact can not be solved without additional conditions *a priori* in a Hertzian manner, no matter how much the solution looks *a posteriori* like Hertzian.

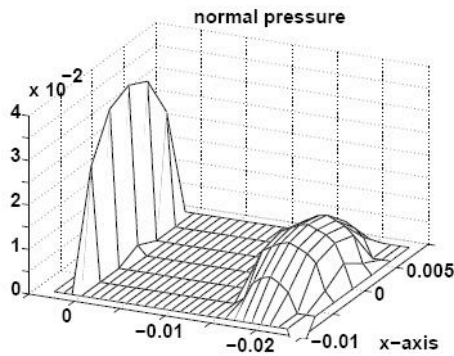
It is also noted that sometimes for certain applications a wheel-rail two-point contact is approximated with Hertzian solution because some additional conditions are found or assumed so that the above mentioned indeterminateness can be resolved. For this deliverable such additional conditions are generally not available.



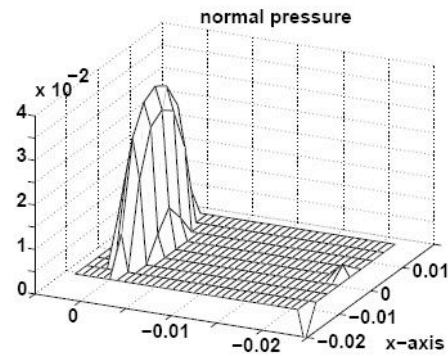
(a)  $\Delta y = 7.50 \text{ mm}$



(b)  $\Delta y = 7.71 \text{ mm}$



(c)  $\Delta y = 7.72 \text{ mm}$



(d)  $\Delta y = 7.96 \text{ mm}$

**Figure 9 - Normal pressure changes when a wheel-rail contact transits from tread-rail top contact ( $\Delta y \leq 7.50 \text{ mm}$ ) to flange-gage corner contact ( $\Delta y \geq 7.96 \text{ mm}$ ). Calculated by WEAR.**

The vertical axis is the contact pressure normalized by the shear modulus of wheel and rail steel  $G = 0.8 \times 10^{11} \text{ Pa}$ . X-axis is in rolling direction. Dimension in the horizontal directions is in meter. The contact area is warped in the lateral direction (horizontal and perpendicular to x-axis), as it is at the gage corner, in the calculation. Here it is presented as being flat. For tangential traction and micro-slip, please see [6].

## 5. Simulation of the lab tests

The methodology presented above is applied to the analyses of the results of the three test rigs.

One of the objectives of this deliverable is to predict the location of the maximal pressure and shear stress. Obviously there can be places at the wheel-rail contact where the pressure and shear stress can be very high but fatigue does not necessarily have to occur due to some reasons, for instance when the wear rate is too high, see discussion in annexes 3 and 4. The maximal pressure and shear stress among all the possible wheel-rail contacts are therefore not necessarily related to RCF. If such stresses are calculated and provided without discretion to subsequent analyses of WP4.3, they may be misleading. Hence the task comes down to the prediction of the maximal pressure and shear stress at locations where fatigue may most probably occur. Because it is shear which causes deformation, the focus is on the shear stress, rather than on the pressure.

For this reason the determination of the location of fatigue initiation and the determination of the associated maximal shear stress are coupled. They are determined in this report by comparison of the shear stress with the shear strength of the material, together with other information available from the measured profiles. The maximal shear stress used is not that among all the possible between the wheel-rail contact, but that in the contact area where based on the analysis fatigue may most probably take place. This appears to be a valid approach as can be seen from the analyses of the tests below. It should be noted that the shear stress has only a relative meaning because the coefficient of friction was not measured in the VAS and DB tests. But owing to the reasons given in section 9 of annex 3, it does not affect the validity of the approach.

### 5.1 The UoN test results

For the UoN test the contact was between two cylindrical discs [1, 2]. The applied maximal pressure was  $p_{z \max} = 1.5 \text{ GPa}$ . The test was conducted in such a way that the first 5,000 cycles were dry<sup>4</sup> with measured coefficient of friction  $\mu$  between 0.4 and 0.45<sup>5</sup>, followed by water drip being applied, with measured coefficient of friction between 0.15 and 0.2. Because the applied slip is  $\xi = 1\%$ , the border between the areas of slip and adhesion in the rectangular contact area is at a distance  $l$  away from the centre of the contact area [8], see figure 10.

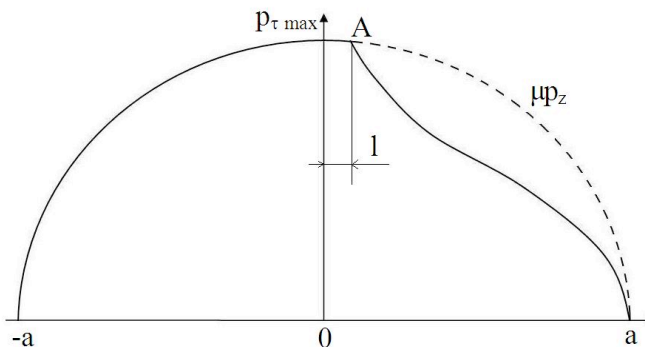


**Figure 10 - Tangential traction distribution between rolling cylinders.  $a$  is the semi-width of the rectangular contact area. The area  $[-a, l]$  is in slip, while  $[l, a]$  is in adhesion.**

<sup>4</sup> The motivation for the first 5000 dry cycles was: (1) To create a more realistic test conditions of mixed dry and wet contacts; (2) To accelerate the initiation of crack to give a realistic while cost effective test duration; (3) Based on experience it was known that it was not likely to produce crack initiation for premium grade with less than roughly 5,000 cycles on SUROS.

<sup>5</sup> Directly measured was the traction coefficient.

$$l = \left[ \frac{\xi E}{2(1-\nu^2)p_{z \max}} \frac{1}{\mu} - 1 \right] a, \quad -a \leq l \leq a$$

For the two steel discs used, Young’s modulus is  $E = 2.1E11$  Pa, Poisson’s ration is  $\nu = 0.28$ . For friction coefficient  $\mu = [0.15, 0.45]$ , we have  $l = [0.69a, a]$ , so that the maximally available shear stress is reached in the contact area and it is

$$p_{i \max} = \mu p_{z \max} = [0.23, 0.68] \text{ GPa}$$

$p_{i \max}$  is theoretically distributed uniformly across the cylindrical surface. For the rail grade R260 (see references [1 and 2]), the ultimate tensile stress is  $\sigma_{u \max} = 0.9$  GPa, so that the ultimate shear stress is

$$\sigma_{s \max} = \sigma_{u \max} \text{Sin}45^\circ = 0.64 \text{ GPa}$$

We have  $p_{i \max} > \sigma_{s \max}$  for  $\mu = 0.45$ .

In applying Hertzian solution for the pressure, the end effect of the cylindrical discs was not taken into account. This may lead to some error in the actual maximal contact stress.

## 5.2 The VAS test

The simulation of the VAS WET 1 test and the analysis of results are presented in annex [3].

## 5.3 The DB rig C test

The simulation of the VAS WET 1 test and the analysis of results are presented in annex [4].

## 5.4 Comparison of results of the three rigs

The three rigs have different complexity; SUROS being the simplest and DB rig C the most complicated.

1. Coefficient of friction (COF,  $\mu$ ): On SUROS a COF of 0.4 – 0.45 was measured for its first 5,000 dry cycles. For both the VAS rig and the DB rig results no COF was measured. Based on observations of HC forming at the VAS rig in relation to water application, and taken into account of the COF measurement on SUROS and the observed higher COF under dry field conditions (up to 0.6), a guess of COF 0.45 is made for the VAS WET #1 test, see annex [3]. For the DB test No. C01, the COF could be between 0.1 and 0.2 due to its constant water application, see annex [4].
2. Based on such COF, the maximal shear stress and the locations are calculated and listed in table 1

**Table 1 - maximal shear stress and locations calculated (in GPa)**

	UoN SUROS	VAS WET 1	DB rig C
Max. shear stress and COF	0.675 ( $\mu = 0.45$ )	0.59 ~ 1.0 ( $\mu = 0.45$ )	0.71 ~ 0.83 ( $\mu = 0.2$ )
Max. shear stress and COF			0.38 ~ 0.47 ( $\mu = 0.1$ )
Location of max shear stress	Across the cylindrical surface	$Y_{\text{cnt}} = 25 \sim 33$ mm. i.e. 3 ~ 11 mm from inner rail side	$Y_{\text{cnt}} = 0 \sim 26$ mm, i.e. 10 ~ 36 mm from inner rail side

0.59 ~ 1.0 means in the range between 0.59 and 1.0 GPa

One can see in the table that with  $\mu = 0.45$  for UoN SUROS and VAS WET 1, and  $\mu = 0.2$  for DB rig C, the maximal shear stress is in the same order. Note the maximal shear stress of R260 material is 0.64 GPa.

3. Under the respective test conditions, the R260 material showed some kind of damage on SUROS, and VAS reported HC on its rig. Although no RCF was reported of the DB test by preliminary inspection, further examination of the DB test sample by Corus revealed some embryonic cracks. The range of the cracks appears to be in agreement with the predicted location of the maximal stress, 10 – 36mm measured from the inner rail side.
4. The above discussion may indicate that although the complexity of the rigs differs, the stress and the damages the materials experienced may be comparable with each other to certain extent under certain load and friction conditions. The extent of their comparability needs be further investigated by subsequent wear, metallurgical, micro-structural and fatigue analyses, and by comparing with operation conditions. The actual RCF behaviour of the tested material may then be determined. It should be emphasized that what is analyzed here is the preliminary results. Further improved tests may provide better comparability.
5. The predicted VAS HC location is between 3 and 11 mm from rail inner side, which is in good agreement with the actual measured HC location of 2 to 8 mm from the rail inner side on the test sample. This part of the rail was first worn into conformal contact before HC initiated. An important explanation for the difference between the prediction and the measurement is the difference in wheel passes: The prediction was based on measured profiles of 20,000 and 50,000 passes, while the measurement of the HC location was performed on the test sample after 100,000 passes. For the DB rig C test, the contact is mainly on top of the rail and part of the gage shoulder, the predicted location of the maximal stress is between 10 and 36 mm from the inner rail side, in agreement with the location of the embryonic cracks on the test sample examined by Corus. The difference in the locations of maximal stress and cracks of the VAS and DB tests reflects the difference in the test conditions.
6. The effective rail inclination of the VAS WET #1 test differed from the design configuration. This should be due to the deformation in the load chain of the rig. The same happened to the DB rig C test; the possible causes may include deformation of the test rig in the load chain, and the way the rail head was fixed on the roller.
7. Although there was deformation in the load chain on the VAS rig, the rail profile measurements are consistent and smooth. This indicates that the test conditions were stable. Consequently the contact conditions around the HC initiation location were stable and the simulation results for the different wheel passes are also consistent. There was no intermediate profile measurement for the DB rig C test. It is therefore not possible to check the consistency by analyzing the profile evolution. It is, however, observed that the measured rail profile had irregularities which should not be due to measurement error. This may be attributed to the factor that the test conditions were not very stable.
8. The maximal shear stress is compared with shear strength of the material to assist the identification of the locations of fatigue crack initiation, together with some other information available from the measured profiles. This appears to be a valid approach. But the maximal shear stress alone is not sufficient.

## 5.5 Some further discussions

The analyses show that:

1. Lack of measurement of friction coefficient, it is difficult to determine purely by numerical method precisely the actual stress level and the resulting RCF consequence. The coefficients of friction for the VAS and DB tests are guessed based on observations and measurements of relevant tests. It is necessary to measure the coefficient of friction.
2. RCF initiation and growth depend not only on the stress level and the material strength, but also on a number of other factors. It is known, for instance, that RCF initiation will be suppressed if the wear rate is high. A complete RCF analysis requires therefore a close collaboration of lab tests, stress analysis, wear analysis, metallurgical analysis, micro-structural analysis, etc.

## 6. Conclusions

---

In this report a methodology for the simulation and analysis of wheel-rail rolling contact is presented. It is then applied to the identification of actual test conditions and to the determination of the contact stress, micro-slip and the location of maximal contact stress of the first laboratory tests conducted in the frame of WP4.3. Subsequently the locations of RCF initiation of the tests are predicted. The predictions are further compared with measurements, namely the actual rail inclination and the locations of RCF cracks. The validity of the methodology is established.

The methodology can be employed for analysis of rolling contact under operational conditions and lab conditions. The results of the analyses can further be used for wear, rolling contact fatigue analyses, etc.

It may also be concluded that for a successful test the test conditions should be controlled and measured so that the test results can be interpreted without uncertainty and can be compared with other tests or with situations under operational contact. Without measurement of the coefficient of friction, the predicted tangential stress has only a relative meaning.

## 7. References

---

- [1] *Initial Definition of Conditions for Testing Matrix of Rail Steels and Welds*, D4.3.1-F2-TESTING\_MATRIX\_DEFINITION.DOC, available in KMS of InnoTrack
- [2] *D4.3.3 Results of first test rig measurements*, available in KMS of InnoTrack
- [3] Kalker JJ (1990), *Three dimensional bodies in rolling contact*, Kluwer Academic Publishers, Dordrecht/Boston/London
- [4] Li, Z. and Kalker, J.J., *The Computation of Wheel-Rail Conformal Contact*, Proc. The 4<sup>th</sup> World Congress on Computational Mechanics, 29 June – 2 July, 1998, Buenos Aires, Argentina
- [5] Li, Z., Kalker, J.J., Wiersma, P.K. and Snijders, E.R., *Non-Hertz Wheel-Rail Wear Simulation in Vehicle Dynamical Systems*, Proc. the 4th International Conference on Railway Bogies and Running Gears, 21 - 23 September, 1998, Budapest, Hungary, 187-196.
- [6] Li, Z., *Wheel-Rail Rolling Contact and Its Application to Wear Simulation*, Ph.D Thesis, TU Delft, 2002
- [7] K.L. Johnson, *Contact Mechanics*, Cambridge University Press, 1985

## 8. Annexes

---

### List of annexes

- [1] Hertzian solution vs non-Hertzian solution, annex 1 to *D4.3.4 Calculation of contact stress*
- [2] Profile smoothing method and calibration, annex 2 to *D4.3.4 Calculation of contact stress*
- [3] Analysis of VAS Wet #1 test results, annex 3 to *D4.3.4 Calculation of contact stress*
- [4] Analysis of the DB test No C 01 results, annex 4 to *D4.3.4 Calculation of contact stress*
- [5] Determination of the effective rail inclination for the VAS Wet #1 test, annex 5 to *D4.3.4 Calculation of contact stress*